Stony Brook University

OFFICIAL COPY

The official electronic file of this thesis or dissertation is maintained by the University Libraries on behalf of The Graduate School at Stony Brook University.

© All Rights Reserved by Author.

Evolution of Surface Morphology and Chemistry in ZnO Thin Films and Steel Surfaces studied by Synchrotron X-ray Spectroscopy and Imaging

A Thesis Presented

by

Hua Jiang

to

The Graduate School

in Partial Fulfillment of the

Requirements

for the Degree of

Master of Science

in

Materials Science and Engineering

Stony Brook University

May 2016

Stony Brook University

The Graduate School

Hua Jiang

We, the thesis committee for the above candidate for the

Master of Science degree, hereby recommend

acceptance of this thesis.

Yu-chen Karen Chen-Wiegart-Thesis advisor

Assistant Physicist, National Synchrotron Light Source II, Brookhaven National Laboratory

Tadanori Koga – Second Reader

Associate Professor, Material Science and Engineering Department, Stony Brook University

Stanislas Petrash– Third Reader

Adhesive Research, Material Science and Engineering, Henkel Adhesive Technologies

This thesis is accepted by the Graduate School

Charles Taber

Dean of the Graduate School

Abstract of the Thesis

Evolution of Surface Morphology and Chemistry ZnO Thin Films and Steel Surfaces studied by Synchrotron X-ray Spectroscopy and Imaging

by

Hua Jiang

Master of Science

in

Materials Science and Engineering

Stony Brook University

2016

Thin film and surface treatment play an important role in developing materials with unique properties. They have been widely used in energy generation and storage, optical devices, LEDS, electrical semiconductor devices, etc. The stability and functionality of them under operational environment are important, especially the surface morphology and chemical evolution at micro-scale. This information is critical to understand the behaviors of the materials under various environments for a wide range of applications. Synchrotron x-ray fluorescence (XRF) and x-ray absorption near edge structure (XANES) are suitable techniques on investigating surface morphology and chemical evolution. Here, we use both techniques to investigate chemical and morphological heterogeneity of zinc oxide thin films after environmental humidity exposure, as well as surface and chemical evolution of iron oxidation states during iron redox process for samples with/without surface anti-corrosion treatment.

Zinc oxide (ZnO) thin films have been reported to suffer from degradation in electrical properties, leading to failure of electronics due to environmental factors, such as heat and humidity. While degradation appears to be linked to water and oxygen penetration in the ZnO film, a direct observation in ZnO film morphological evolution, in conjunction with structural and chemical changes is lacking. Here, we systematically investigated the chemical and morphological heterogeneity of ZnO thin films caused by steam treatment. X-ray fluorescence microscopy, absorption spectroscopy, grazing incident small angle and wide angle scattering, scanning electron microscopy (SEM), ultra-high-resolution SEM and optical microscopy were carried out to examine ZnO, Al-doped ZnO and Ga-doped ZnO thin films, on two different substrates – silicon wafer and PET film. The environmental aging introduced pin-holes in the un-doped ZnO thin film. More significant morphological features formed in the Al-doped ZnO thin films after treatment, with platelet-shaped structures that are 100-200 nm wide by 1μm long. In addition, Zn heterogeneity, anisotropic structure and disordering were also observed in the aged Al-doped ZnO thin films using synchrotron x-ray characterization. X-ray diffraction and absorption spectroscopy indicate the formation of a zinc hydroxide in Al-doped films due to environmental aging. Utilizing advanced characterization methods, our studies provide information with unprecedented level of details and reveal the chemical and morphologically heterogeneous nature of degradation in ZnO films.

Anti-corrosion coating is widely used on industrial steel products. While the effect of these coatings is proven to be positive, fundamental studies on the chemical evolution of the protected metal is lacking. Here, we conducted *in situ* x-ray spectroscopic experiment to observe the process of steel corrosion with and without the protective coating. X-ray fluorescence mapping was conducted to observe surface morphology and elemental distribution during redox

process. X-ray absorption near-edge structure spectroscopy was performed to determine the oxidation states and chemical information of Fe. Steel without coating was corroded rapidly and homogeneously, within 1 hour. Steel with anti-corrosion Zr-based (Henkel Corporation) coating showed good resistivity to corrosive environment (5wt% NaCl solution). Only very slight local oxidation was observed after approximately 10 hours of treatment. Our study laid foundation for possibility to conduct *in situ* research on numerous materials under various environments.

Table of Contents

List of Figures

List of table

Acknowledgments

First, I want to thank my advisor at Brookhaven National Laboratory, Dr. Yu-chen Karen Chen-Wiegart. Your support and encourage during the past year helped me a lot. I was always able to learn from the discussion with you. It is your inspiration and guidance that helped me gain all the scientific skills. I'm always grateful for all the comments and revision you made on my manuscripts, posters, and presentations.

I also want to thank Dr. Stanislas Petrash, the project leader from Henkel. Your passion and guidance helped me a lot. Thank you for bringing these two great projects so that I have the opportunity to take part in them. Your effort in conducting ultra-high resolution SEM and your comments on my manuscripts and posters are greatly appreciated. I'm also grateful for Dr. Kang Wei Chou from Henkel. Thank you for providing comments on my manuscripts and conducting experiment.

I am also grateful to NSLSII faculty Juergen Thieme, Garth Williams, and Lisa Miller. With your guidance, the life is much easier in BNL. I really learned a lot from your professional spirit.

I would like to express my gratitude to Professor Tad Koga. Thank you for your support and constructive comments on my manuscript.

I definitely want to thank the other member Chonghang Zhao in Karen's Group. Thank you for bringing much information to me through the past year. The discussion with you is always interesting and helpful.

I want to thank Kim Kisslinger (CFN) for iron sample preparation. Thank Mingyuan Ge (NSLSII) for providing the *in situ* cell and pumper. Thank Evgeny Nazaretski (NSLSII) for

redesigning the holder of *in situ* cell. Thank Yong Chu (NSLSII) for his excellent ideas on *in situ* experiments. Thank Li Li (NSLSII) for analysis software PyXRF. Thank Syed Khalid (NSLSII) for helping in Athena. Thank Paz Carreras (Henkel Ibérica S.A.) for the preparation of the zinc oxide films used in this work. Thank Gwen Wright (CFN) and Fernando Camino (CFN) for help in the SEM training, Mingzhao Liu (CFN) for training and assisting in the sputter coating of zinc oxide. I want to thank Hanfei Yan, Wen Hu, Xiaojing Huang, from NSLSII for comments on my practice presentation in BNL.

I want to thank all SRX supporting staff- technical support: James Biancarosa, Michael Maklary, Carey Koleda (NSLSII); control support: Wayne Lewis, Tommy Tang, Mechanical support: Yuan Yao (previous NSLSII, now IBM), Michael Lucas and Richard Gambella (NSLSII).

Use of the National Synchrotron Light Source II, Brookhaven National Laboratory, was supported by the U.S. Department of Energy, Office of Science, Office of Basic Energy Sciences, under Contract No. DE-SC0012704.

This research used resources of the Center for Functional Nanomaterials, which is a U.S. DOE Office of Science Facility, at Brookhaven National Laboratory under Contract No. DE-SC0012704.

The Advanced Light Source is supported by the Director, Office of Science, Office of Basic Energy Sciences, of the U.S. Department of Energy under Contract No. DE-AC02-05CH11231.

Finally, I want to thank my family, especially my parents, who gave me support and love during my two years study. I’m grateful that they provided me the opportunity to study in Stony Brook University.

Chapter 1. Introduction

1.1 Motivation and goals

Coating is one of the most widely used surface treatments. Functional coating may be applied to change the surface properties such as adhesion, corrosion resistance, or wear resistance[1]. Various materials processes can be used to fabricate coatings: chemical vapor deposition (CVD), physical vapor deposition (PVD), spraying, sputtering and other techniques. The parameters in coating processes and the intrinsic material properties of the coatings vary significantly. All these combined to result in the different properties and end applications of each coating. The films and their desired properties may degrade under environmental conditions, such as heat, humidity and corrosive environments. Understanding the changes of the properties for the coating or the protected materials under these conditions is of great importance both for the applications and for the fundamental research. In this dissertation work, with the capability of synchrotron source x-ray fluorescence (XRF) and x-ray absorption near-edge structure (XANES) at the National Synchrotron Light Source II, we focus on exploring the surface and chemical heterogeneity in coatings and their protected materials.

The thesis outlines as following. First, we aim to understand the long-term stability of ZnO thin film, and explain the degradation phenomenon by investigating the chemical and morphological heterogeneity of ZnO thin film after humidity exposure. By conducting the research on ZnO thin film, it helps to understand the relationship between degradation in micro scale with electrical/optical changes in macro scale. Secondly, we studied the functionality of a phosphate-free anti-corrosion coating (Henkel Corporation) by monitoring steel corrosion with in situ x-ray measurements. We developed *in situ* x-ray fluorescence (XRF) and x-ray absorption

near-edge structure (XANES) capability which helped lay foundation of conducting *in situ* research on numerous materials under gas/liquid flow environments. In the future, with our researches, we have the potential to explain the properties of not only coating materials but a wider range of materials under controlled environment by visually "see" the changes with XRF and XANES in an *in situ* cell. The techniques used in this research are described briefly in the following.

1.2 X-ray and synchrotron sources

Since the discovery of x-ray in 1895, x-ray has become a powerful probe of the structure of matter. X-rays can be used to detect a wide range of materials, from simple compounds to complex structure such as DNA[2]. Our understanding of the way x-rays interact with matter developed steadily. The main limitation of x-rays was the source. In the 1970s scientists found that the synchrotron radiation emitted from charged particles circulating in storage rings was potentially a much more intense and versatile source of x-rays[3]. Due to the ability to produce x-rays with high brilliance, many synchrotrons were designed especially for the installation of wigglers and undulators and with beam optics of extremely low emittances. Some of "third generation" machines providing the required long straight sections are currently under construction[3].

1.3 X-ray absorption near-edge structure (XANES)

The absorption cross-section for photoexcitation of a core-electron to vacuum is not a smooth function, but exhibits oscillations near the absorption edge. This signal is referred to as near-edge x-ray absorption fine structure (NEXAFS) or x-ray absorption near-edge structure (XANES) [2].

After an x-ray photon is absorbed by a core level, a photoelectron is generated. This photoelectron might not be ejected into the vacuum due to the lack of energy to be promoted to an unoccupied but bound level [2, 4-6]. The core hole caused by the absorption process can be filled either by an Auger process or by capture of an electron from another shell followed by emission of a fluorescent photon [2, 4, 5]. The differences between XANES and traditional photoemission experiments are that in the latter, the initial photoelectron itself is measured, while in XANES the fluorescent photon, Auger electron or inelastically scattered photoelectron is recorded. In photoemission spectroscopy only excitations beyond the ionization threshold are possible to be detected. For XANES, the final state of bound photoelectrons can be measured, since the photoelectron itself need not be detected [2, 4, 5]. Hence, the effect of measuring fluorescent photons, Auger electrons and directly emitted electrons is to sum over all possible final states of the photoelectrons, which means that what XANES measures is the total density of states of the initial core level with all final states[2, 5].

XANES is able to determine the chemical form due to the differences in spectra of different valence state for the same element. In our study of iron oxidation, XANES is sensitive to Fe redox states, especially the pre-edge feature, which is located ~14-20 eV the main K-edge crest of Fe. Pre-edges are related to 1s to 3d and/or 1s to 4p transition. As oxidation state increases, pre-edge shifts to higher energy. Depending on the oxidation states of Fe, the spectra can vary significantly. By comparing the spectra with shoes taken on standards, we are able to determine the oxidation states of Fe. Thus, XANES is a suited method to determine the redox status of Fe.

1.4 X-ray fluorescence

X-ray fluorescence (XRF) records the spectral response of the emitted photos produced by relaxation of excited states formed by photo absorption at a given incident energy [2, 4, 5]. It is an ideal method for determining the elemental composition of objects that are either too thick for transmission-absorption measurements, or are insulating and therefore preclude photoemission techniques. XRF is widely used in archaeology, geochemistry, and even used to investigate elements of paint[2]. The Schematic of x-ray fluorescence spectroscopy of the setup available at Sub-micron Resolution X-ray Spectroscopy Beamline at National Synchrotron Light Source – II is shown in Figure 1, with a focus size of sub-micron. The setup can also be used to collect XANES spectra in fluorescence mode.

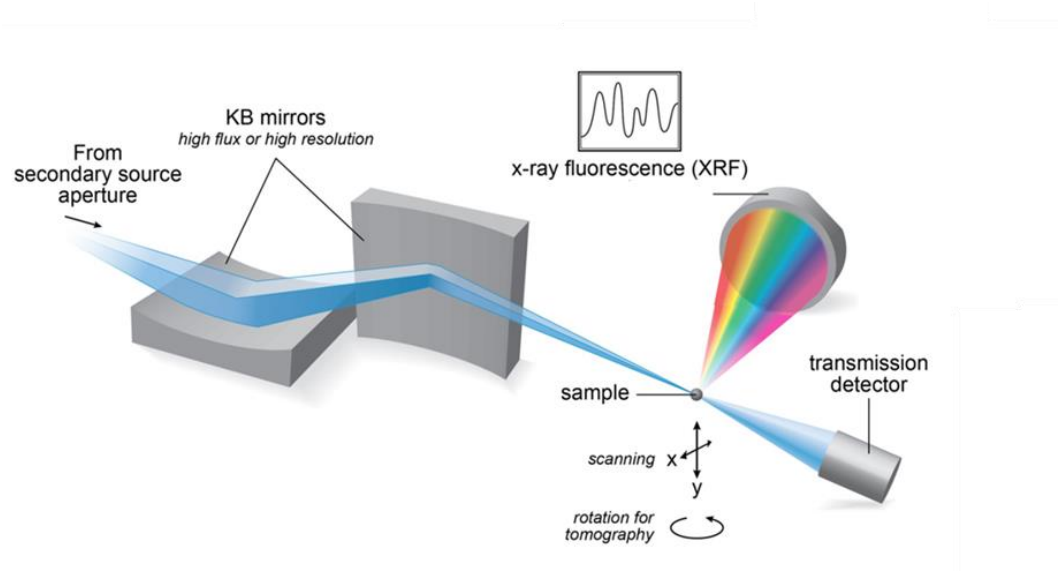

Figure 1 Schematic of x-ray fluorescence spectroscopy setup

Chapter 2. Chemical and Morphological Heterogeneity of Zinc Oxide Thin Films after Environmental Humidity Exposure

2.1. Introduction

Zinc oxide (ZnO) possesses many unique properties and attracts great attention in both fundamental research and industrial applications, , particularly in the as various nano-structures, such as nano-wires [7, 8], nanobelts, nanohelices [9] and thin films [10, 11]. Zinc oxide applications are wide and versatile, ranging from conventional electronics, solar cells [12-14], humidity sensors, to emerging applications in chemical energy technologies [15], piezoelectric nanogenerators [16], energy scavenging [17], and electromechanically coupled sensors [9]. In many applications, increased electrical conductivity is desirable, which is usually achieved by doping of ZnO with other elements. In particular, Al-doped ZnO, has a high conductivity, as well as good optical transmission properties in the visible and near infrared range. Thus, Al-doped ZnO is considered suitable for applications that require both transparency and electrical conductivity such as organic light-emitting devices [11] and solar cells [18, 19]. However, ZnO thin films, especially with Al-dopants, are not stable under harsh environment such as elevated heat, humidity and UV exposure, which limits the applicability of ZnO-based materials in devices requiring long-term stability [20]. Therefore, it is important to understand the long-term stability and degradation phenomena in ZnO thin films. Most of the studies on ZnO thin films focus on structural, electrical, optical properties and sensing abilities [12-14, 20-29], but only a few report on chemical and morphological changes of ZnO under environmental treatment such as high temperature and high humidity, (so-called damp heat treatment). Influence of deposition methods, film thickness, dopant and film quality on the degradation of ZnO films under damp heat treatment were previously studied [12, 21-23, 30]. In general, a decrease in resistivity,

mobility and carrier density was reported [23] for Al-doped ZnO thin film after damp heat treatment. Penetration of water and oxygen along the grain boundaries and formation of $Zn(OH)_2$ were reported to be responsible for the degradation of electrical and optical properties [20, 23, 25, 26]. It has been previously reported that when an Al-doped zinc oxide thin film is subjected to damp heat treatment, the surface of the film exhibits morphological heterogeneity, where large and small spots were formed for samples treated with high temperature (100°C) and high humidity (100% relative humidity) [12, 27]. However, the nature of this heterogeneity, such as chemical and elemental compositions, remained unclear, lacking particularly the detailed morphological analysis.

In this thesis work, we focus on studying the chemical and morphological heterogeneity of ZnO thin films when the materials are subjected to steam treatment and compare it with the untreated pristine samples. A wide range of techniques were utilized to characterize the pristine and aged samples. The elemental distribution in the thin film was characterized by x-ray fluorescence. The chemical evolution was studied by x-ray absorption near edge structure spectroscopy. The crystal structure was investigated by x-ray diffraction, whereas grazing-incidence wide-angle x-ray scattering and grazing-incidence small-angle x-ray scattering were used to determine the mid-to-long range ordering. Optical and scanning electron microscopies were also performed to characterize the morphology of the samples.

2.2 Methods

2.2.1 Sample preparation

ZnO thin film samples were manufactured through RF magnetron sputtering (ATC-ORION 8 HV system, AJA International, Inc.) at room temperature (conditions see Supplemental Materials Table S1). Two different substrates were used to study the effect of substrates: Silicon wafer (P

type B-doped Si, <100> cutting orientation, 500 μm thick, 4 inch wafer from University Wafers) and Polyethylene terephthalate (PET) film (clear, untreated CUS5 Autostat). To study the effects of dopants, thin film samples with three different compositions were prepared separately by using different sputtering targets: ZnO, aluminum doped ZnO (Al:ZnO) and Gallium doped ZnO (Ga:ZnO).The thickness of the thin film is 50 nm for Al:ZnO and Ga:ZnO, 60 nm for ZnO. Small square pieces of thin film samples were cut; the length of each side for the square samples is 2.5 cm.

2.2.2 Aging Treatment

Pristine samples were first characterized by the techniques detailed below, and were then treated to purposely introduce degradation. Water vapor treatment was carried out to age the samples where an environment of 100% relative humidity at 100°C was created to simulate the harsh environment under an accelerated aging condition. Introducing conditions of both high humidity and elevated temperature to perform aging is widely adapted in academic research and industrial testing [12, 21, 23, 26, 30], which is also addressed as ‘damp heat’ treatment, or ‘accelerated aging’. To perform the water vapor treatment, a 500 mL beaker was filled up with deionized water and the water surface kept to 3 cm from the top of the beaker. The beaker was then covered by 2 pieces of glass slides with about 2 cm in between and heated with a hot plate until boiling. The samples were then placed on top of the glass slides with the coated side facing directly the boiling water vapor for 1 hour (Figure 2).

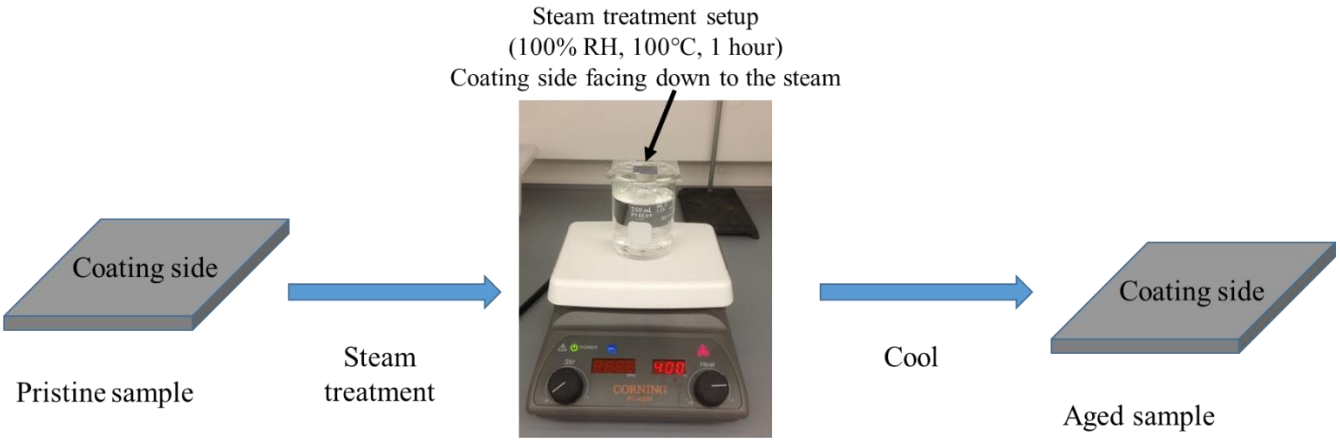

Figure 2 process of sample treatment

2.2.3 Characterization

By comparing the results from the treated samples and the pristine ones we aim to study the environment induced heterogeneity in coating materials. The pristine and treated samples were each characterized to study the morphological and chemical evolution. Optical Microscopy (OM) was used. Scanning Electron Microscopy (SEM, Joel 7600F) and Energy Dispersive X-ray Spectroscopy (EDS, Joel 7600F) were used to characterize the surface morphology and chemical distribution. X-ray diffraction (XRD) measurements were performed (Rigaku Ultima III) to investigate the chemical and structural changes. OM, SEM, EDS and XRD were performed at the Center for Functional Nanomaterials (CFN) of the Brookhaven National Laboratory (BNL). XRF and XANES measurements were carried out by utilizing the Sub-micron Resolution X-ray Spectroscopy (SRX) beamline at the National Synchrotron Light Source II of BNL. XRF 2D element mapping was used to observe the morphology of the film surface and XANES was used to verify the chemical change before and after the treatment. Grazing incidence x-ray scattering (small angle and wide angle) measurements (GISAXS and GIWAXS, respectively) were performed at beamline 7.3.3 at the Advanced Light Source, Lawrence Berkeley National

Laboratory. A PILATUS 2M from Dectris was used to collect the scattering patterns. The sample-to-detector-distance was set to 0.224 m (GIWAXS) and 3.806 m (GISAXS), respectively. A conic flight tube under vacuum was placed between the sample and detector, to reduce air scattering. A shallow angle of 0.26 degrees was chosen for the incident x-rays – above the critical angle of the inorganic films – with respect to the sample plane. The width of the incident x-ray beam is about 1 mm and silver behenate was used to calibrate the lengths in the reciprocal space.

2.3 Results

2.3.1 Morphological analysis of ZnO thin films

ZnO, Al-doped ZnO and Ga-doped ZnO thin films were investigated before and after treatment with 100 % relative humidity at 100° C. All thin films were prepared with two different substrates: Si wafer and PET film. For both ZnO and Ga-doped ZnO on Si and PET substrates after treatment, little morphological change was observed with optical microscopy and scanning electron microscopy (SEM). In contrast, for Al-doped ZnO on both Si and PET substrate, significant morphological changes were observed in the treated sample compared with the pristine one. Figure 3(a-b) show the surface morphology of pristine and aged Al-doped ZnO thin films on the Si substrate observed by optical microscopy (OM). For the pristine samples, the surface morphology is homogeneous, while bright and dark regions were formed in the aged sample, with crack-like structures observed in both regions. Figure 3(c-d) show survey SEM images of the pristine and aged Al-doped ZnO films on the Si substrate. The film displays a homogeneous surface morphology before treatment (Figure 3c). Flake-like platelets with bright contrast (marked by blue arrows in Figure 3d) and dark contrast (marked by red arrows in Figure 3d) were formed after the treatment, which are also observed in the film grown on the PET

substrates, as shown in Figure 3(e-f). The size of the bright-contrast plates is ~100-200 nm wide by 1 μm long. The bright and dark platelets with are believed to be the same type of platelets, with dark and light SEM contrast arising as a result of different orientations. , The darker platelets lie on the surface, being better connected to the partially-conductive substrate, while brighter plates are oriented perpendicularly to the surface of the thin film (and therefore are subject to well-known "edge effect". Furthermore, the contact area of these plates with the surface are much smaller compared to the ones that are parallel to the surface. The smaller contact area may cause higher charging of the plates which results in a brighter contrast in the SEM images.

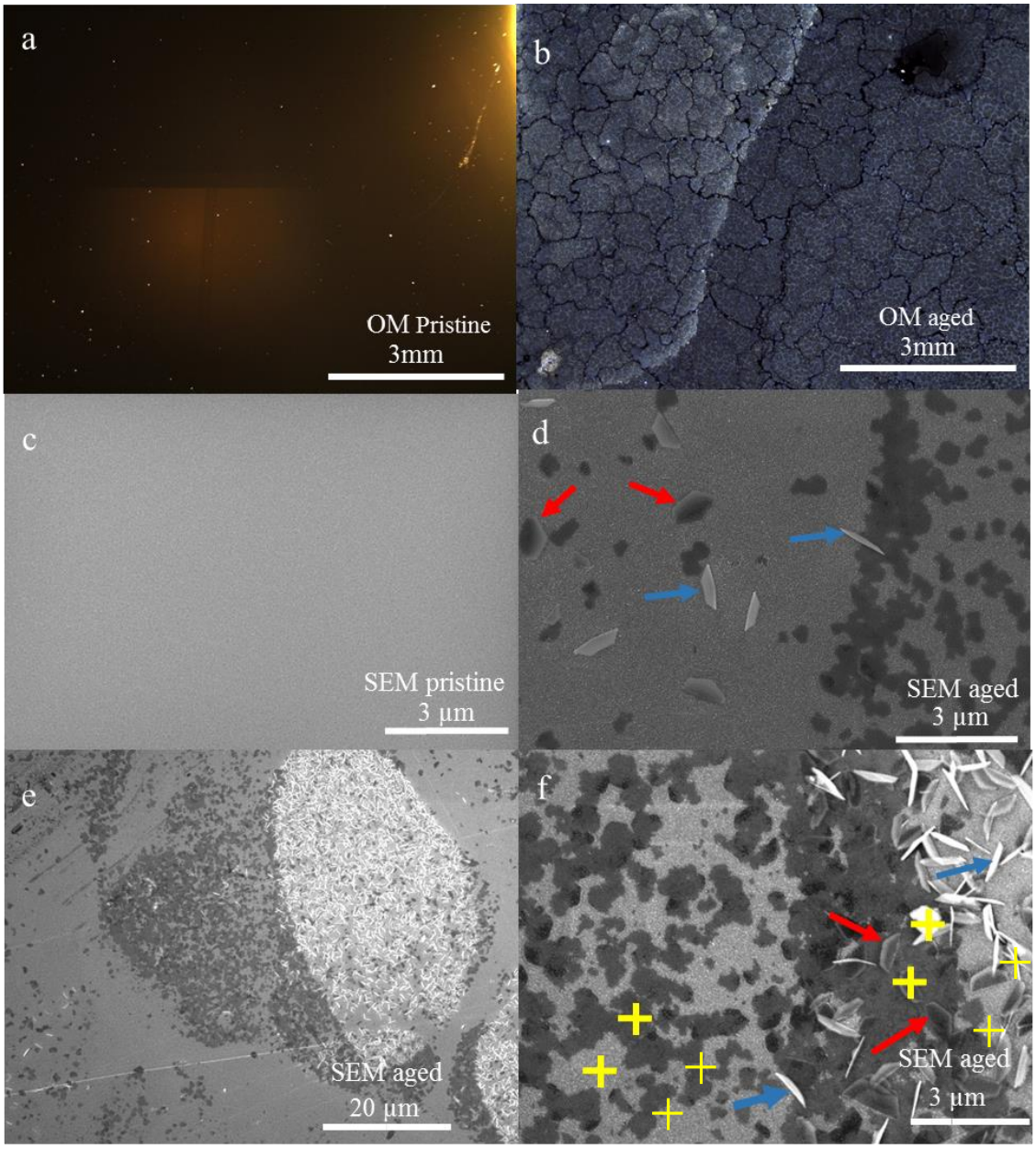

Figure 3 Optical images of Al-doped ZnO films on a Si substrate: (a) pristine (b) aged; SEM images of Al-doped ZnO films on a Si substrate: (c) pristine (d) aged; (e-f) SEM images of aged Al-doped ZnO films on a PET substrate for two different magnifications, respectively.

Electron dispersive spectroscopy (EDS) measurements were performed on selective positions (marked with yellow crosses) in the SEM images (Figure 3f) for elemental analysis,

and EDS mapping was performed in the entire region shown in Figure 3f. The elemental compositions in areas with brighter and darker contrast plates, as well as regular areas have been investigated (supplemental materials –Table S2). No evident elemental differences were detected amongst the entire films in EDS, while the expected elements (O, Zn, Al, Si, C) were detected from either the sample composition or the sample mounting. These results show that the Zn and O are the major components of the plate-shaped structures created during the water vapor treatment. However, an overall reduction in Zn quantity was observed after the treatment in Al-doped ZnO sample on the PET substrate with higher Zn content in the plate-shaped structures.

To further study the morphological changes upon aging in undoped and Al-doped ZnO films on a finer scale, the ultra-high resolution SEM studies have been performed, using Hitachi SU9000 SEM. A unique feature of this instrument is an energy filter on the top high-angular back-scattered electron (HA-BSE) detector, which was used to enhance the contrast originating from the crystallinity and the orientation of ZnO features on the surface.

Figure 4(a-b) shows the secondary-electron (SE) and high-angular back-scattered electron (HA-BSE) image with energy filtering, correspondingly. Unlike SE image, which only shows morphological contrast, HA-BSE image shows many of the ZnO grains in untreated sample appearing brighter, due to their orientation towards the detector (positioned coaxially to incident electron beam). In the SEM images collected from the treated sample (Figure 4 (c-d)), the HA-BSE image (Figure 4d) shows that considerably fewer number of ZnO grains appear as brighter, suggesting that treatment causes reduction in crystalline ordering and orientation of the crystal grains (see also GISAXS section).

Further investigation also shows clear evidence of pinhole formation as a result of steam exposure. Figure 4f and g shows SEM images for untreated and treated samples, correspondingly. An imaging mode utilizing beam deceleration feature was used (with landing voltage 1.5kV), to increase the sensitivity to surface features. The SEM image of the treated sample clearly shows pinholes ~10nm in size, as well as deeper, more pronounced gaps between individual ZnO grains, which causes a reduction of overall structural ordering. This may also lead to potential mechanical instability and reduction in conductivity, leading to device degradation. A decrease of the film crystal ordering was also seen after aging, as observed in Figure 4d where fewer grains were highlighted in the energy filtered SEM image. However, no plate-shaped structures were formed in the ZnO film, in contrary to the Al-doped ZnO film shown previously. Figure 4(e-f) show ultra-high resolution SEM images of the pristine and aged Al-doped ZnO films on the Si substrate. The detailed view of the plates formed due to aging confirms that the plates with brighter and darker contrast were the same type of features, with different orientations. Considering the process of water condensation on the film surface during the water vapor treatment and water drying, it is likely that the water droplets during drying caused the plates to align along different orientations. The plates were also found to be rough on the surface with additional features, which cannot be seen in the regular SEM.

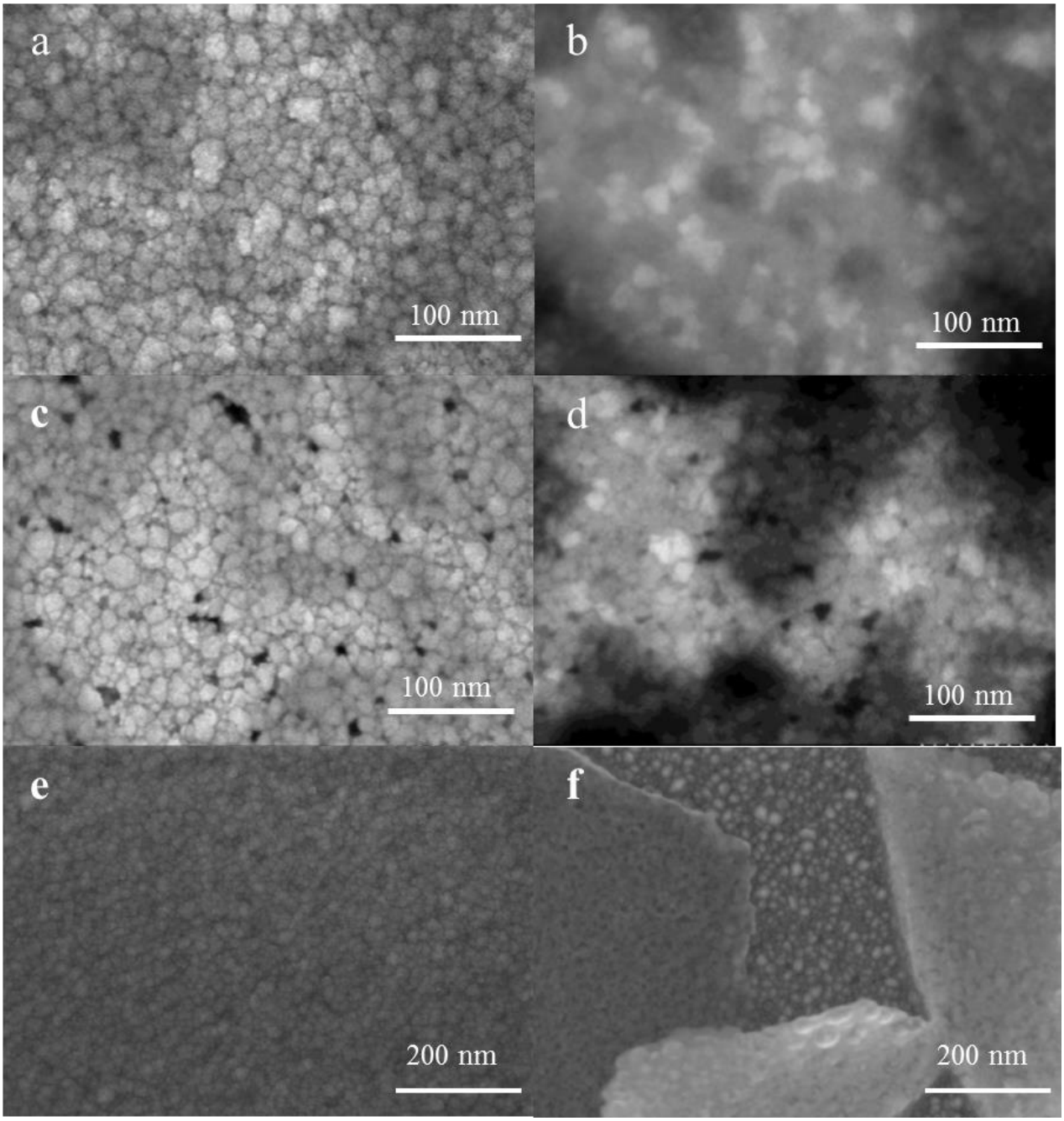

Figure 4 Ultra high resolution SEM images of ZnO films on a Si substrate: pristine sample (a) without energy filtering (b) with energy filtering; aged sample (c) without energy filtering (d) with energy filtering. Al-doped ZnO films on a Si substrate: (e) pristine sample (f) aged sample.

2.3.2 Crystal Structure analysis

The crystal structure of the film before and after treatment was studied by x-ray diffraction which was carried out on all the samples grown on a Si substrate. The bare Si wafer was also measured as a reference. Figure 5 shows the XRD results of the pristine and aged Al-doped ZnO thin films. The Si (400) peak from the substrate appears at 69.2°, consistent with the surface cut of the substrate. The peak at 34.4° corresponds well with ZnO (002). An additional peak appears at 23.3° which is only present in the aged Al-doped ZnO thin film. The $Zn(OH)_2$ peak was previously reported to appear at 23.35° after steam treatment [20]. Thus, the additional peak from the aged Al-doped ZnO is considered to be $Zn(OH)_2$. It is reported that water can be absorbed at the grain boundaries of ZnO and forms $Zn(OH)_2$[8, 14, 17]. All other peaks are also present in the bare Si wafer and are thus considered to be originating from the substrate. The rocking curve was measured with a ± 0.3° angular range on all the peaks from the Si wafer (32.9°, 54.6°, 56.4°, 61.7°, 65.9°, 66.4° and 69.2°, see Figure 7 in the supplemental material) and the intensity change was recorded as a function of the sample surface angle relative to the incident x-ray beam. The high angular sensitivity confirms that the peaks correspond to the substrate itself, and therefore are highly textural.

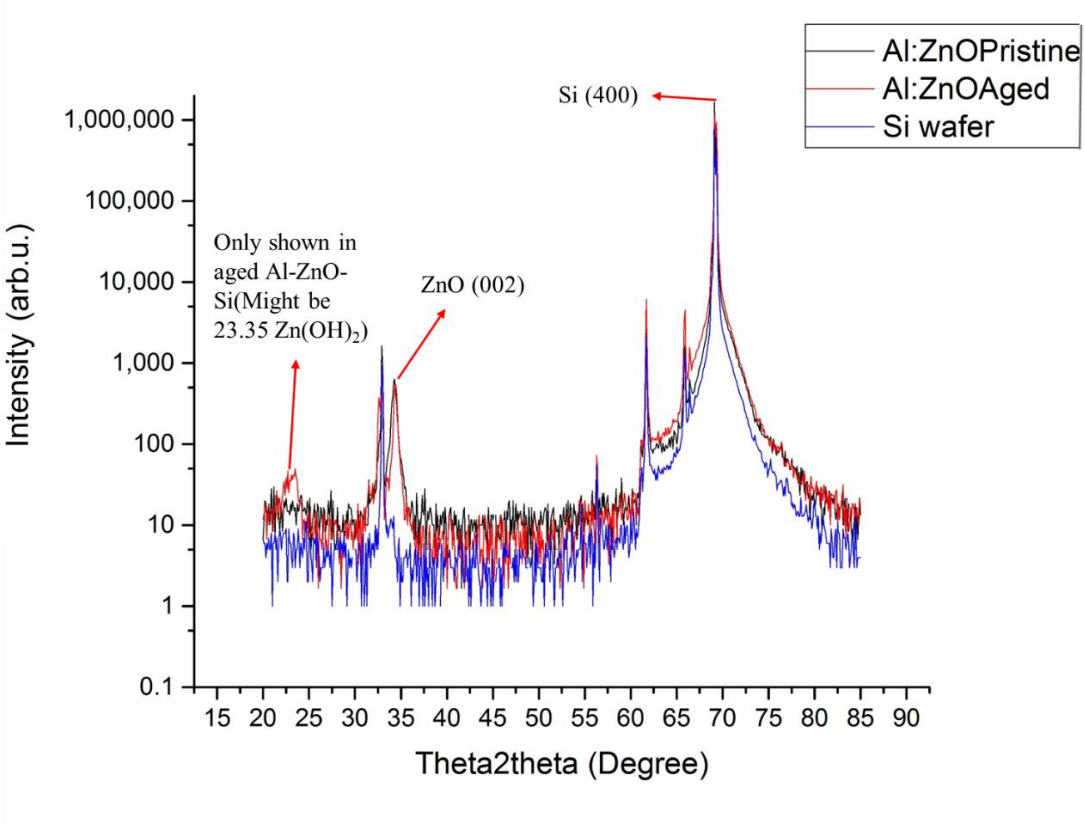

Figure 5 XRD pattern of pristine and aged Al-doped ZnO on a Si substrate and the bare Si wafer.

The crystallinity and grain size of the inorganic thin films were also studied by means of grazing incidence wide and small angle x-ray scattering (GIWAXS and GISAXS), respectively. Both techniques provide information about the lateral and normal ordering at a surface or inside a thin film and require smooth films on a flat substrate. Therefore, only the films deposited on a silicon wafer as substrate were studied here. The measurements were performed with an incidence angle of 0.26° and the energy of the x-rays was set to 10 keV. Figure 6 shows the raw 2D GIWAXS patterns for the ZnO films undoped and doped with Al and Ga, before and after steam treatment, respectively. The different crystal planes are indicated as well. The distance between the lattice planes of the main peak, corresponding to the (002) crystal planes is 0.259 nm. Surprisingly, a very anisotropic crystal structure forms for the Al doped film after steam

treatment with a lamellar d spacing of about 0.773 nm, which may correspond with the plate-shaped structure and zinc hydroxide formation, as described above.

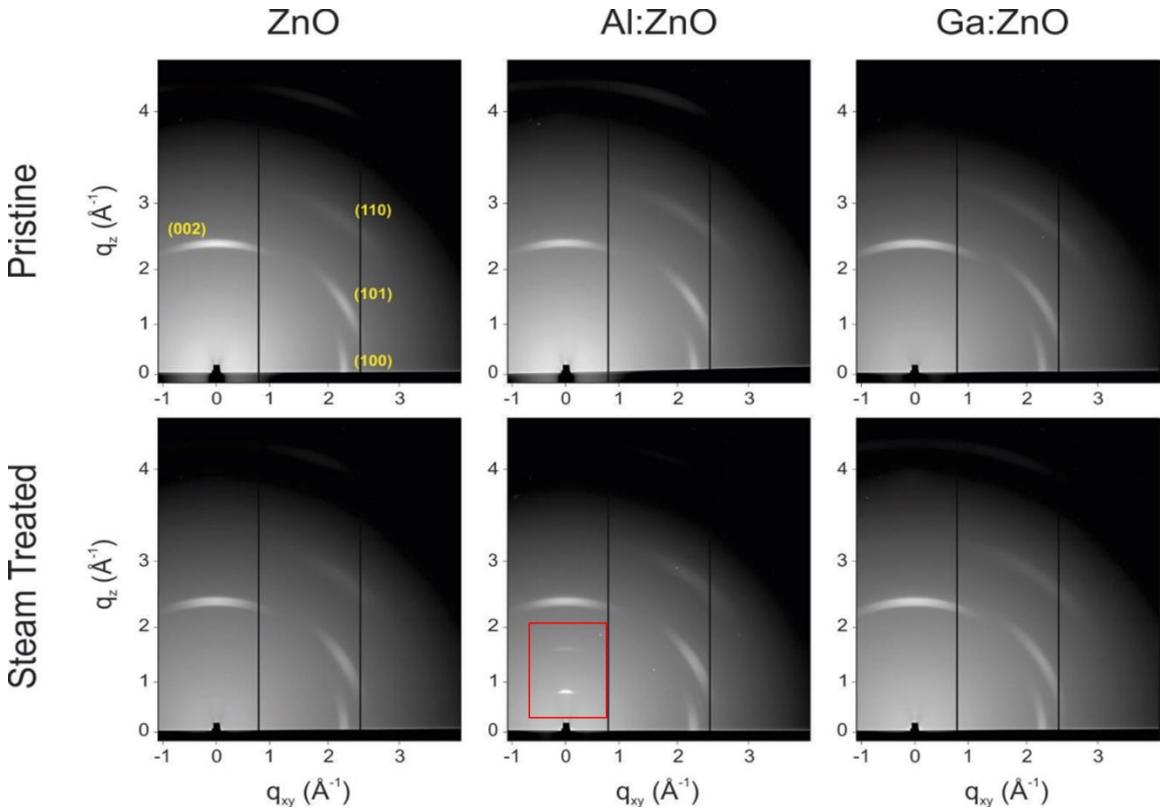

Figure 6 2D GIWAXS patterns of the ZnO films, undoped and doped with Al and Ga, before and after steam treatment. An anisotropic structure was only observed in Al-doped ZnO, highlighted by the red rectangle.

An example GISAXS pattern is shown in Figure 7a for the pristine ZnO film. The yellow box indicates the integration area and in order to evaluate the in-plane ordering, a vertical integration is performed. The resulting line cuts for all films are summarized in Figure 7b. The positions of the shoulders provide information on the domain size. These domain sizes most likely correspond to the grain sizes of the films, as observed by the high-resolution SEM data (see Figure 4). The in-plane domain size is about 38 nm for the ZnO film, 39 nm for the Al

doped ZnO, and 21 nm for the Ga doped ZnO. After steam treatment, a flattening can be observed of the line cuts, indicating a reduction in ordering. This is consistent with the high resolution SEM data, where the pinholes form and grain ordering on the surface of the homogeneous pristine thin films appears to degrade after steam treatment.

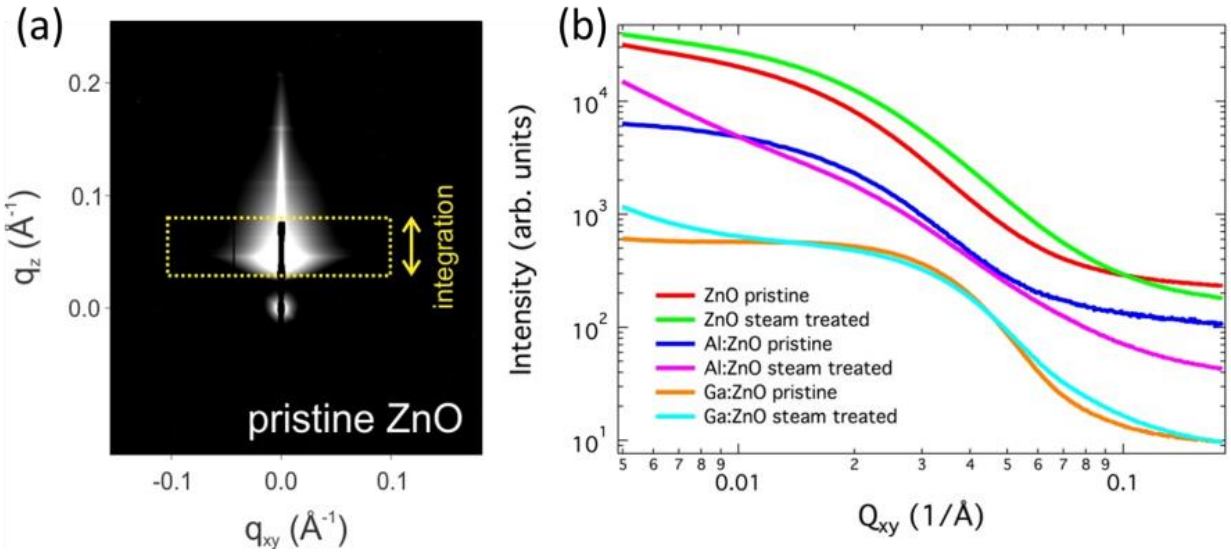

Figure 7 (a) raw GISAXS pattern of pristine ZnO without steam treatment. The yellow box with double-arrow indicates the integration area and direction. (b) The resulting line-cuts following the same procedure for all ZnO films, undoped and doped with Al and Ga, before and after steam treatment.

2.3.3 Synchrotron-based X-ray Absorption Spectroscopy Chemical Analysis

Scanning micro- x-ray fluorescence (XRF) mapping of the Zn distribution was collected on ZnO and Al doped ZnO on the PET substrate before and after treatment. Little changes were observed in the in ZnO on the PET substrate after treatment (Figure 8 (a-b)). In contrast, the Zn spatial heterogeneity is clearly evident developed in the treated Al-doped ZnO on the PET substrate, consistent with the SEM results as shown in Figure 3. For the pristine Al doped ZnO on the PET

substrate (Figure 8 c), the image shows that the Zn is homogeneous across the entire scanned region of interest. Spatial heterogeneity of Zn is observed for the aged Al doped ZnO (Figure 8d). This heterogeneity is further confirmed by scanning a larger region of interest on the sample, as shown in (Figure 8e). Higher Zn concentration regions with a size of 20-30 μm were observed, which is about the size of the clusters of the plate-shaped structures observed with SEM, as shown in Figure 3. There is a reduction of the Zn concentration for the Al-doped ZnO film after steam treatment, which is also observed in the ZnO film, consistent with the EDS analysis. This may be attributed to the mechanical instability of the films deposited on the PET substrates which leads to loss of thin film material after steam treatment.

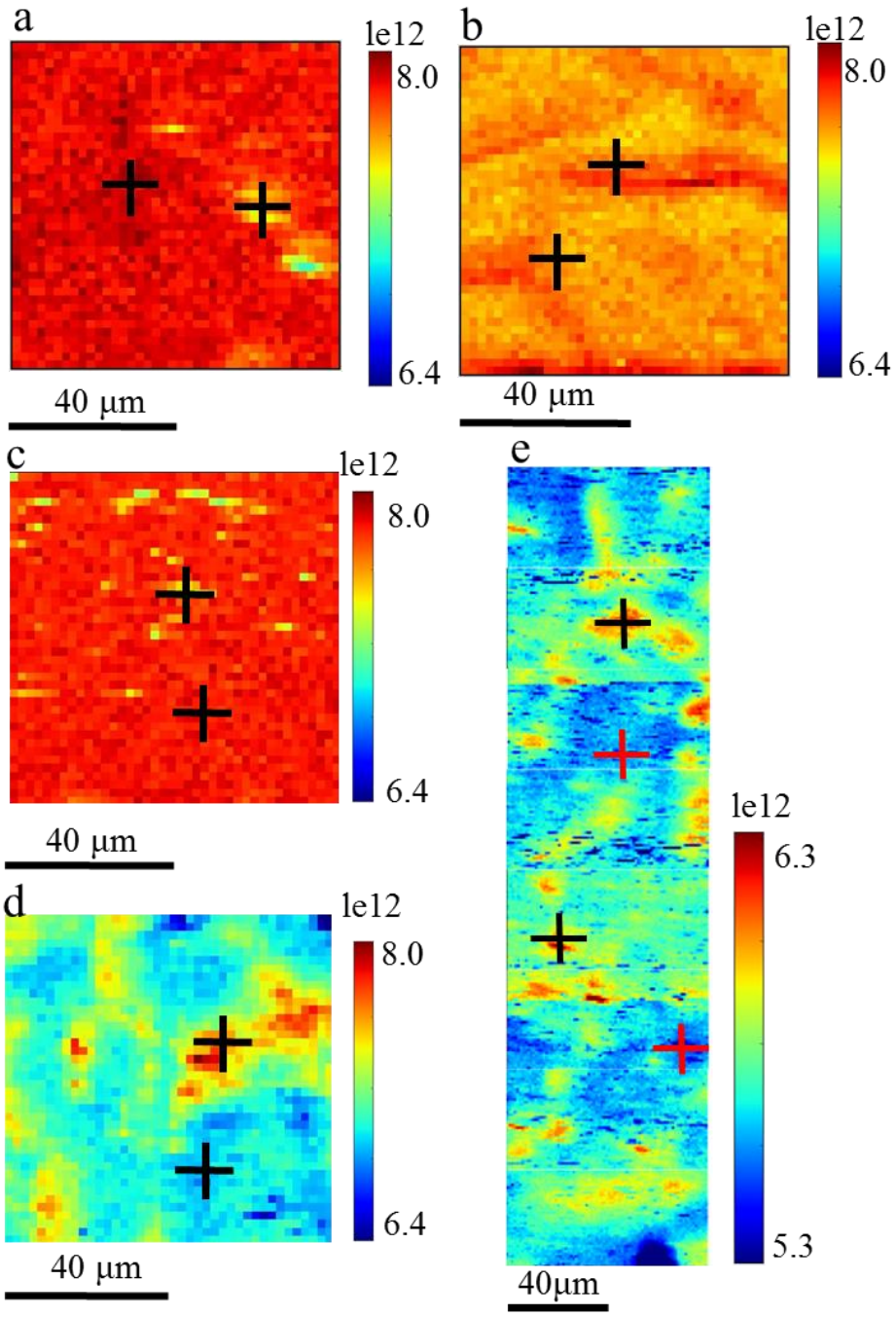

Figure 8 XRF 2-D elemental mapping results: ZnO on PET substrate (a) pristine and (b) aged; Al-doped ZnO on PET (c) pristine and (d-e) aged.

Micro x-ray absorption near edge structure (x-ray absorption near edge structure d.aged; Al-doped e (abuted to the mechanical instability of the films deposited on the PET substratecentrations of Zn on the XRF 2-D maps. As no clear differences could be observed in the XANES spectra between the different points from the same sample, the corresponding spectra were averaged and are shown in Figure 9. Both ZnO and Al-doped ZnO on the PET substrate before and after treatment showed almost no differences in the XANES spectra. Although, according to the literature [31], XANES spectra of ZnO and $Zn(OH)_2$ are nearly identical, in combination with the XRD data, our results indicate the formation of $Zn(OH)_2$ in the aged Al-doped ZnO thin film.

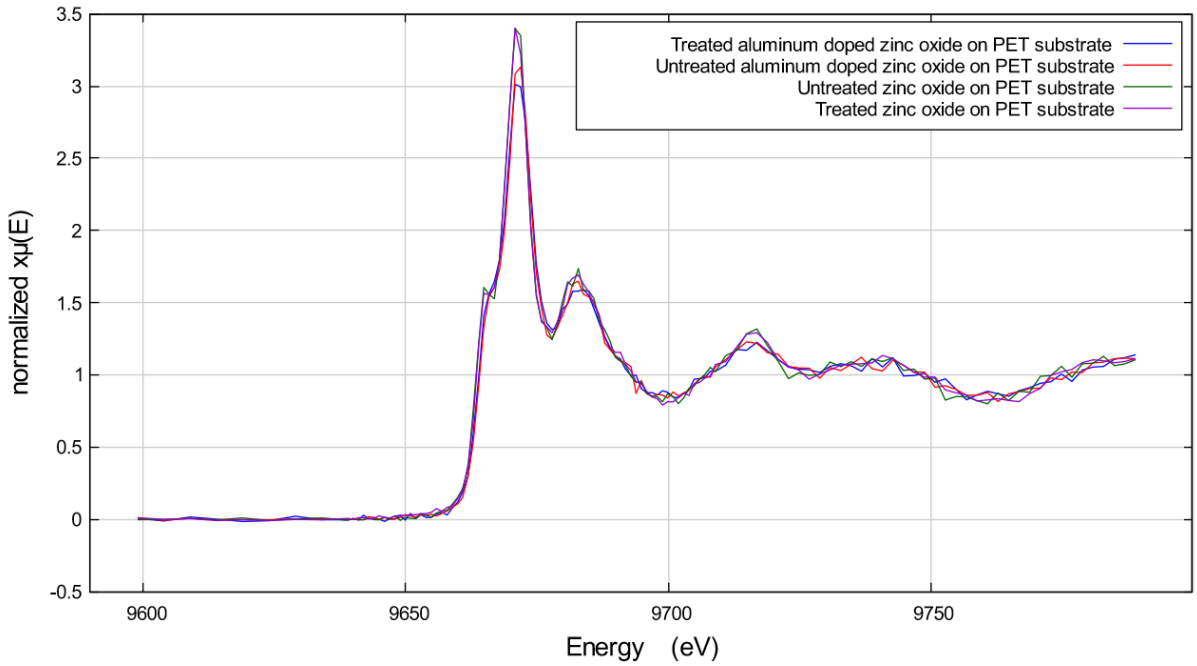

Figure 9 XANES spectra of ZnO and Al doped ZnO thin films on the PET substrate, before and after steam treatment.

2.4 Conclusions

We systematically investigated the degradation of ZnO thin films (un-doped, Al-doped and Ga-doped) on Si and PET substrates due to environmental factors. ZnO and Ga-doped ZnO exhibit only slight morphological changes after aging. Al-doped ZnO on both the Si and PET substrates showed significant morphological changes caused by steam treatment. Platelet-like structures in different orientations, likely to be containing $Zn(OH)_2$ were formed in Al-doped ZnO on both the Si and PET substrates. Ultra-high resolution SEM, GISAXS and GIWAXS revealed the reduction of ordering in the structure and formation of the pinhioles in the thin films after treatment. In particular, a highly anisotropic structure was found in the GISAXS study, likely corresponding to the formation of the plate-like structures formed in the Al-doped ZnO films. A reduction in Zn quantity was observed in both EDS and XRF microscopy, with a higher heterogeneity of Zn observed by XRF in the aged Al-doped ZnO sample. The XANES data is consistent with the XRD results, indicating that the structure can be a mixture of ZnO and $Zn(OH)_2$.

To summarize, the development of pinholes and structural disordering in all ZnO thin films, with in addition the plate-shaped structure and $Zn(OH)_2$ formation in Al-doped ZnO are believed to be predominant mechanism of degradation and is likely main cause failure of the Al-doped ZnO-based devices. As per our study, for the first time, the degradation mechanism was studied in light of morphological and chemical evolution. Advanced synchrotron techniques like XRF, XANES, GISAXS and GIWAXS were used for the first time to characterize degradation mechanism of ZnO films under steam treatment.

Chapter 3. *In situ* Investigation of Surface Morphology and Oxidation States during Iron Oxidation in Steels with Anti-corrosion Coatings

3.1. Introduction

When metallic materials are exposed to corrosive environment, they tend to have chemical reactions with air or water. The corrosion effect is usually evident on the material surface. Metals lacking anti-corrosion protections may rust depends on the level of their exposure to the air. Anti-corrosion coating is one of the most common and efficient ways to protect metals form rusting. It prevents metal from direction contact with air and water, so that it can slow down the rust process dramatically. The understanding of how well these coating work is crucial in corrosion control.

Surface pretreatment are used on metal surface before application of organic paints and finishes for better adhesion and improved corrosion protection[1]. Phosphate conversion coatings have been the most commonly used surface pretreatments for ferrous and non-ferrous metals[1]. However, because of drawbacks from environmental, energy and process standpoints, phosphate conversion coatings are being replaced by alternatives. A new surface pretreatment based on hexafluorozirconic acid solution (introduced by Henkel Corp.) is used as a replacement of phosphating process. The treatment process is phosphate-free, can be applied by simple spray or immersion at room temperature, and does not require chromic acid sealing[1]. The bath is based on diluted H_2ZrF_6 (Zr<200 mg/l) with small quantities of non-hazardous components of Si and Cu added for better long-term performance[1]. 20 nm think anti-corrosion coating will form after the pretreatment. The functionality of the coating is studied by monitoring the iron oxidation states when samples with coating are exposed to corrosive environment.

This study presents the evolution of iron oxidation of steel characterized as a function of time by using *in situ* cell. The cell is designed to conduct x-ray fluorescence (XRF) and x-ray absorption near-edge structure spectroscopy (XANES), and it allows gas or liquid flowing through the pipes and fill up the space where sample is mounted. In our study, sodium chloride solution is used to flow through the pipes, creating a corrosive environment. The elemental distribution in the thin steel sample was characterized by XRF mapping. Micro Fe K-edge XANES spectra were used to determine the oxidation states evolution with sub-micron spatial resolution. Pristine samples were tested. XRF and XANES were performed every 10 minutes to detect corrosion behavior. By conducting the *in situ* measurement, we observed the differences in surface morphology and chemical evolution during iron oxidation with and without anti-corrosive coating (Zr-based solution treatment) under controlled corrosive environment.

3.2 Experiment setup

3.2.1 Sample Preparation

Three steel samples with different protective coatings were prepared to study iron oxidation with different anti-corrosion treatment conditions. Sample 1 was a steel sample with coated commercially available anti-corrosion coating, however without further treatment details available. This sample was prepared mainly for testing purpose. Sample 2 was a steel sample without coating, which serves as a control sample. Sample 3 was a steel sample with Zr-based anti-corrosion coating prepared by solution surface treatment (Henkel Corporation). A summary of all three samples are provided in **Error! Reference source not found.**. All three samples were prepared with the same steal for direct comparison.

Sample 1	Sample 2	Sample 3
Commercial steel with standard anti-corrosion coating (for testing)	Steel without coating (Control sample)	Steel with Zr-based anti-corrosion coating (prepared by surface treatment)

Table 1 Sample information

3.2.2 *In Situ* Flow Cell Design and Assembling

The core of the *in situ* cell assembling consist of two silicon nitride window chips (with two difference sizes, called small and large here), together with O rings and spacers to define the space for liquid or gas to flow through. For both large and small chips, they have one side which is Si with a small window, and silicon nitride (SiN) membrane on the other side which is known as the flat side. All 3 samples were cut into a 30×30 ×1 μm^3 in size under focused ion beam (FIB), with the 1 μm along the beam direction. The samples are then welded with FIB-SEM lift-out and micro-manipulation to the edge of Si_3N_4 window with Platinum (Pt) on the flat side of small chip (**Error! Reference source not found.**). Si_3N_4 window is of the size of 200μm long and 60μm wide. As marked by blue arrows (**Error! Reference source not found.**b), spacers (white) are used to define the path (dark color) in between where liquid or gas can flow through. Right before samples were assembled into *in situ* cell under microscope, both large and small chips shall be cleaned by plasma cleaning to ensure the surface of the chip is hydrophilic and can be wet by the flow.

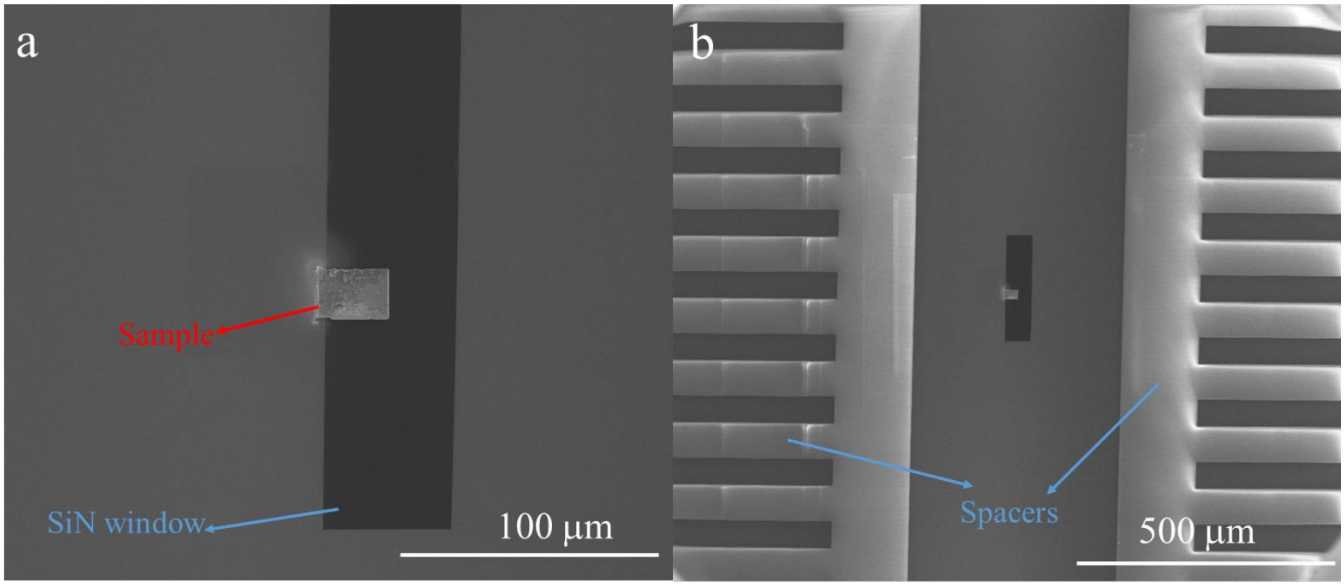

Figure 10 FIB-SEM image of welded steel sample on SiN window of small chip

3.2.3 Corrosion Test prior to *In Situ* Experiment

To test the corrosion condition and ensure that the corrosion reaction can be observed during the time frame of the beamtime, (on the order or hours, not days), test experiments were carried out. Sodium chloride (NaCl) solution with three different concentration (3wt%, 5wt% and 8wt%) were used to treat steel samples. The test result indicates that the 5wt% NaCl is an ideal concentration to be used to treat samples.

3.2.4 *In Situ* X-ray Spectroscopy Experiment

The *in situ* cell and chips which carry the FIBed sample were assembled and placed at the SRX beamline. Few quick XRF mapping with 2 µm step were first done at 18.2 keV to locate the position of sample and confirm the possible elements. Then fine scan of XRF with 1 µm step at 8 keV was conducted before XANES. Points of interest were selected based on fine scan of XRF mapping. *In situ* XANES were done on points of interest.

The treatment was carried out by injecting a 5wt% NaCl solution by a syringe-pump, with tubing connected to the *in situ* cell assembling. The syringe was assembled on the pumper (**Error! Reference source not found.**a-b). The total volume injected into the syringe is 600 μl, and the pumping speed was 1.5 μ/min.

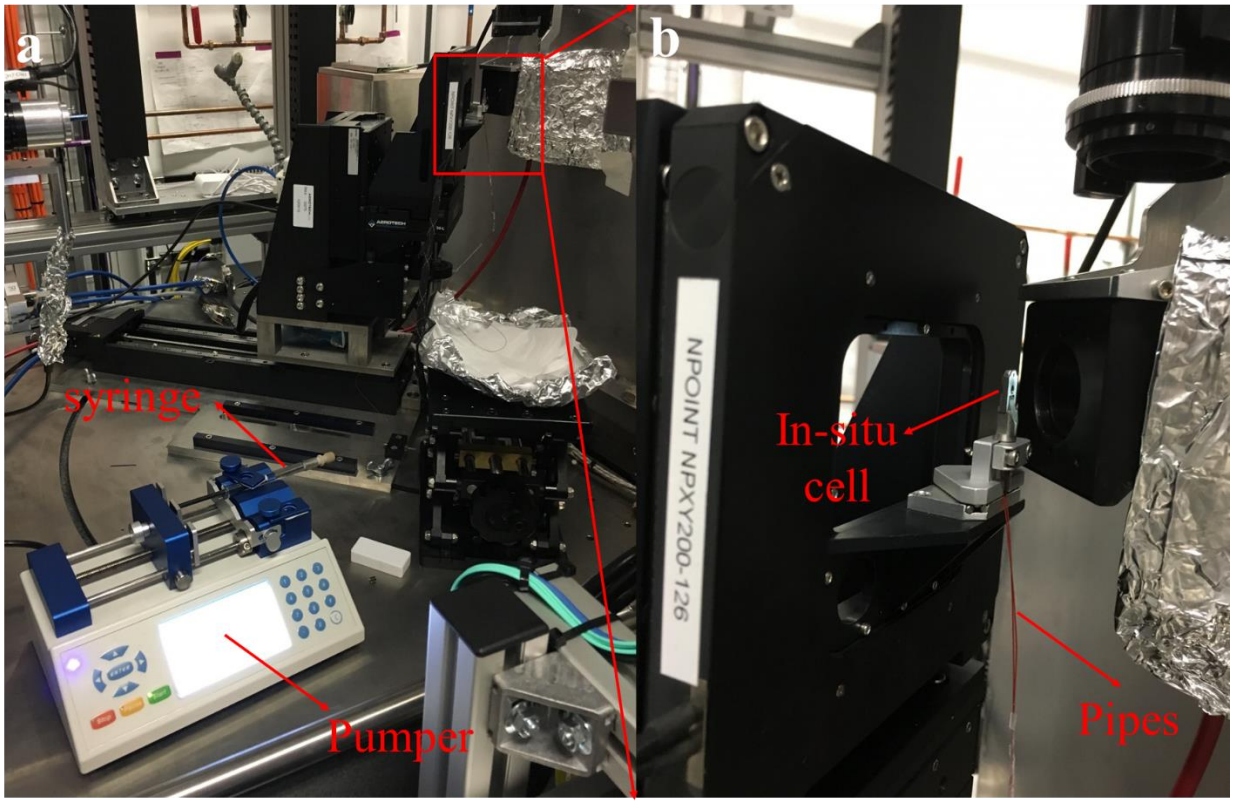

Figure 11 Experiment setup for iron corrosion

3.3 Results

For sample 1 (test sample), it was discovered that due to the lack of plasma-treatment on the chips, solution was unable to wet the interior of the cell assembling. This illustrates the importance of the plasma cleaning treatment. The following section will focus on comparing the result from the control sample (Sample 2) and Zr-based treated sample (Sample 3).

3.3.1 XRF element mapping

For sample 2 (control sample), Cr, Cu, Fe, Ga, Mn, Ni, Pt, Ti, Zn, Zr were found in XRF element fitting. The Ti frame of the *in situ* cell may account for the presence of Ti, and Pt was used to weld sample. XRF mapping of pristine sample 2 was shown in **Error! Reference source not found.**, and treated sample after 0.5 hour treatment in **Error! Reference source not found.**. By comparing **Error! Reference source not found.** and **Error! Reference source not found.**, Fe, Cr, and Mn exhibited morphological changes. All Fe, Cr, and Mn showed lower intensity after treatment. Sample shape changed after the treatment, probably because porous structure formed on sample surface after iron oxidation and was washed away by flowing solution. This may also responsible for the reduction of Fe, Cr and Mn after the treatment.

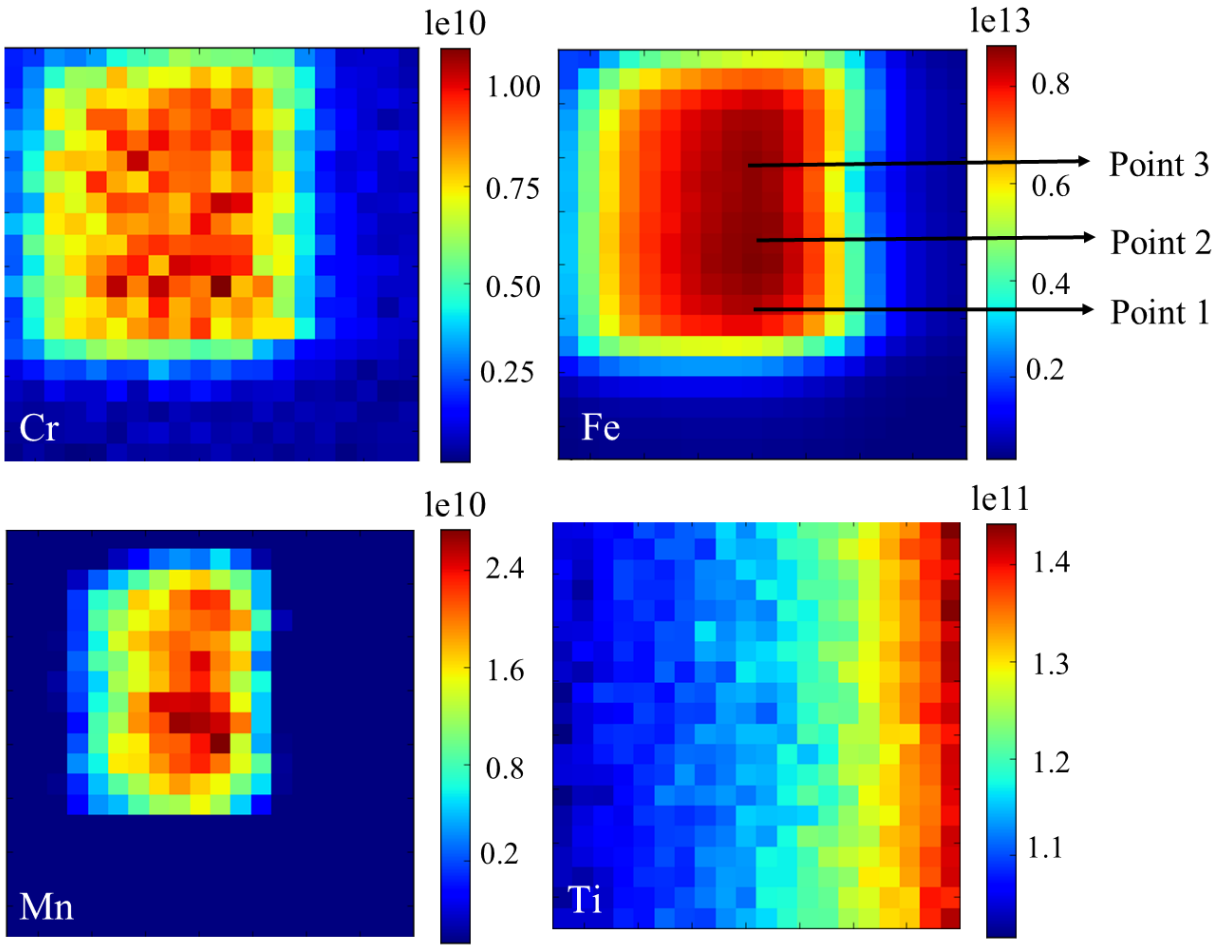

Figure 12 XRF element mapping of pristine sample 2 (control sample)

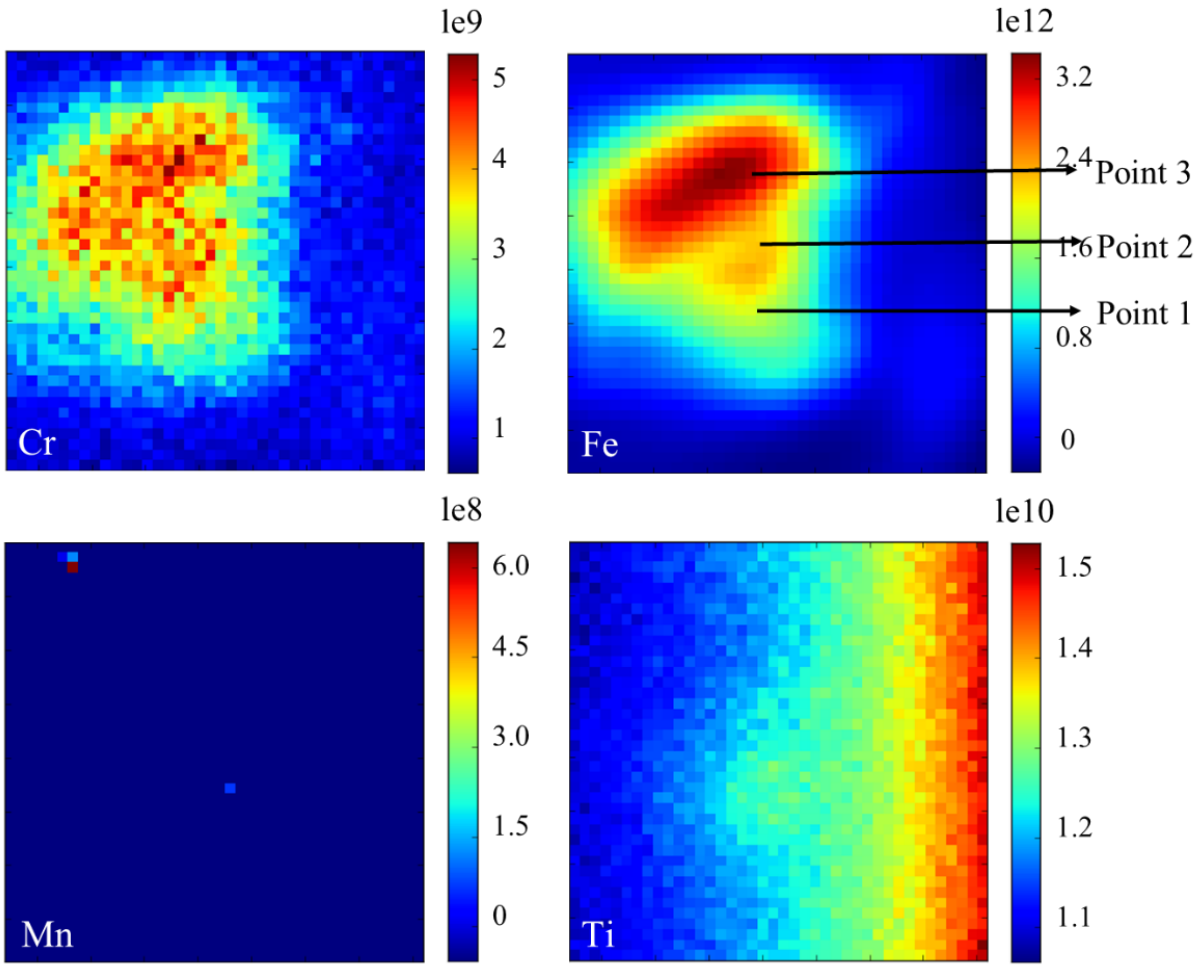

Figure 13 XRF element mapping of treated sample 2 after 0.5 hour (control sample)

For sample 3 (Zr-based treated sample to prevent surface corrosion), Cr, Cu, Fe, Ca, Kr, Mn, Ni, Pt, Ti, Zn, Zr were found in element fitting. XRF mapping of pristine sample 3 is shown in **Error! Reference source not found.**, and **Error! Reference source not found.** showed element mapping of sample 3 after a 12-hour treatment. As shown in the figures, Fe map exhibited slight morphology changes. Concentration of Fe almost remain the same. Cr existed morphological changes, and Mn concentration dropped. From XRF results, no significant morphological or elemental concentration changes were identified. This highlights the

effectiveness of the surface treatment in comparison with the untreated sample 2 where great morphological changes were observed.

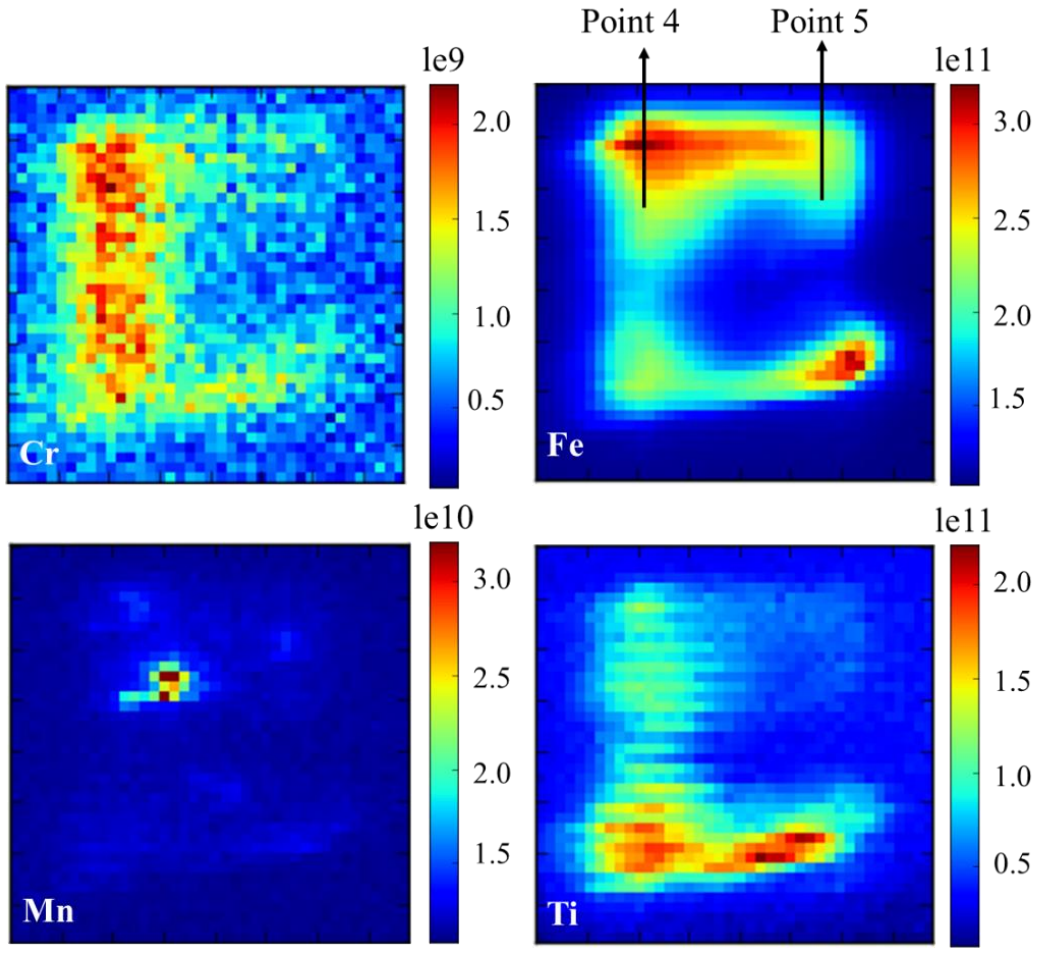

Figure 14 XRF element mapping of pristine sample 3

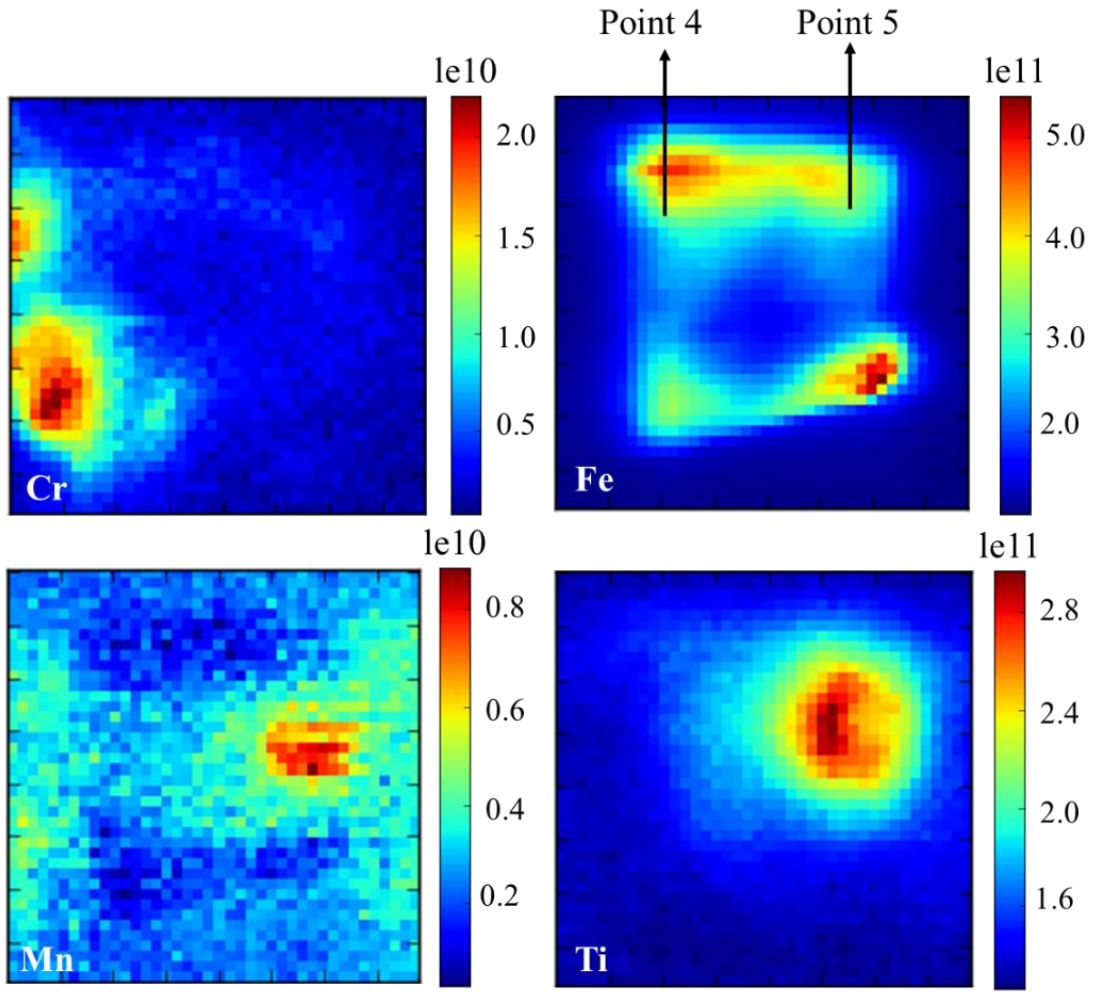

Figure 15 XRF element mapping of treated sample 3 after 12 hours

3.3.2 XANES spectra

As shown in **Error! Reference source not found.**, pristine and treated XANES results were averaged by spectra collected from point 1, point 2, and point 3 shown in **Error! Reference source not found.** and **Error! Reference source not found.**. Point 1-3 from **Error! Reference source not found.** and **Error! Reference source not found.** are at the same location, but XANES test were conducted before (pristine) and after treatment (0.5 hr and 1 hr) respectively. The XANES spectra from the standard powder samples, Fe_3O_4, Fe_2O_3, and FeO, are also

presented. XANES spectra showed that pristine sample 2 is consistent with Fe (0), as expected in steel prior to corrosion. After 0.5 hour treatment, the pre-edge and white peak shifted and intensity increased. Compared with iron and iron oxide standards, at this stage, the spectra start to show a mix of Fe and iron oxides. After 1 hour treatment, pre-edge and white peak shifted greatly towards Fe_3O_4 and Fe_2O_3, and Fe pre-edge structure disappeared. Peak intensity of the white line continuously increased, indicating a nearly complete oxidation of the steel. The result clearly showed the corrosion and oxidation of steel in the solution, demonstrating the feasibility of *in situ* cell setup.

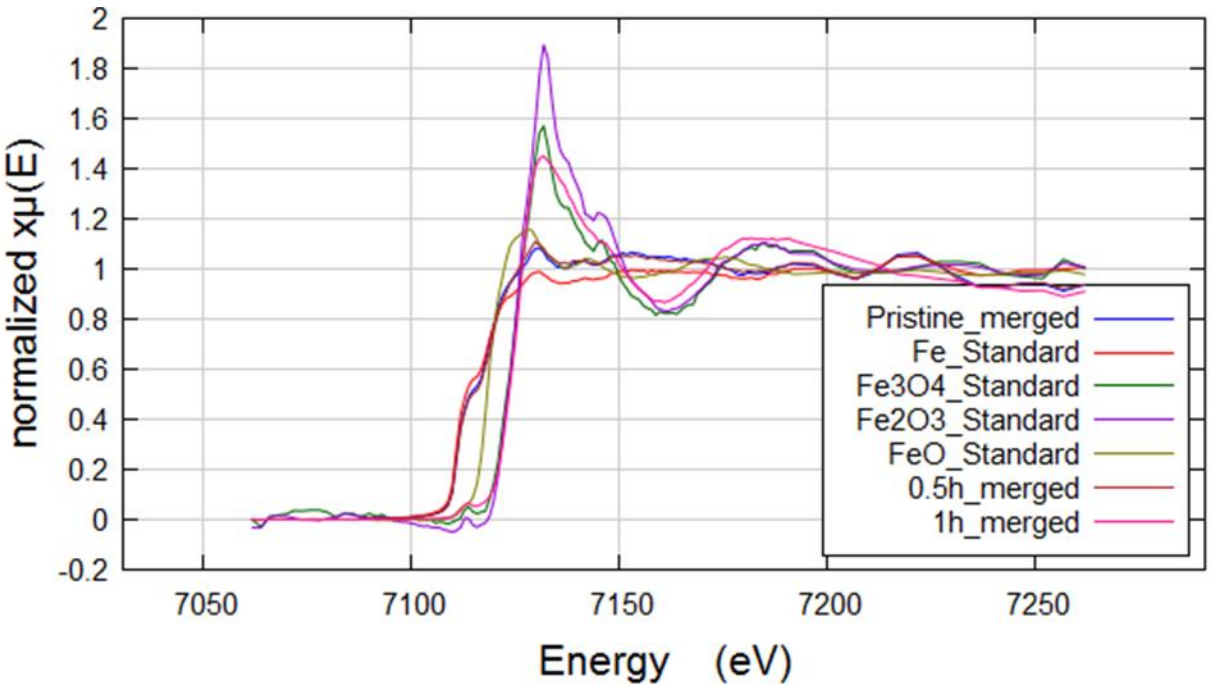

Figure 16 XANES spectra of pristine and treated sample 2 in comparison with Fe standard compounds

For sample 3, as shown in **Error! Reference source not found.**, XANES spectroscopy was conducted from point 4 and point 5 from locations shown in **Error! Reference source not found.** and **Error! Reference source not found.**. The very first scan of both point 4 and point 5

represented the scans on the pristine sample (**Error! Reference source not found.**). The time between each scan for both points is 20 minutes. Sample 3 exhibits a unique double peak XANES spectra which is different form Fe standard, though it still shows similar pre-edge structure as existed in Fe spectra. This may because during the process of surface treatment, the surface reacts with the Zr-based coating materials and formed a layer of different type of Fe compound. By comparing every spectra collected from point 4, no systematical changes were observe. In other worlds, compared with XRF mapping (Figure 14 and Figure 15), no oxidation was detected at point 4. However, when comparing spectra from point 5, it showed that there were systematical intensity increase for the white line, especially the last few scans (**Error! Reference source not found.**a). Though the intensity increase is not less pronounced in comparison with the un-treated sample, it might link to the slow oxidation process occurred at point 5.

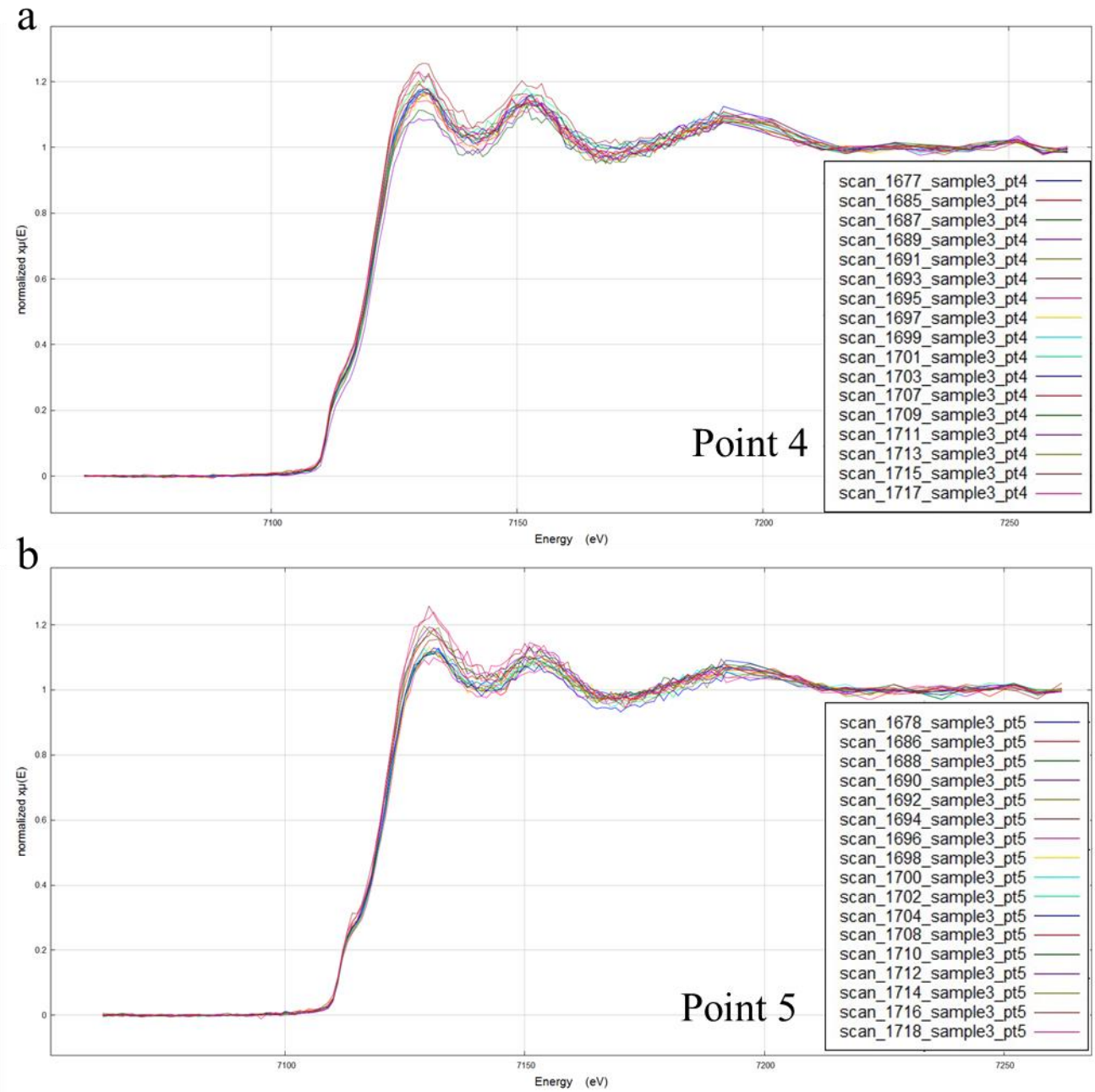

Figure 17 a. XANES spectra of sample 3 point 4. b. XANES spectra of sample 3 point 5

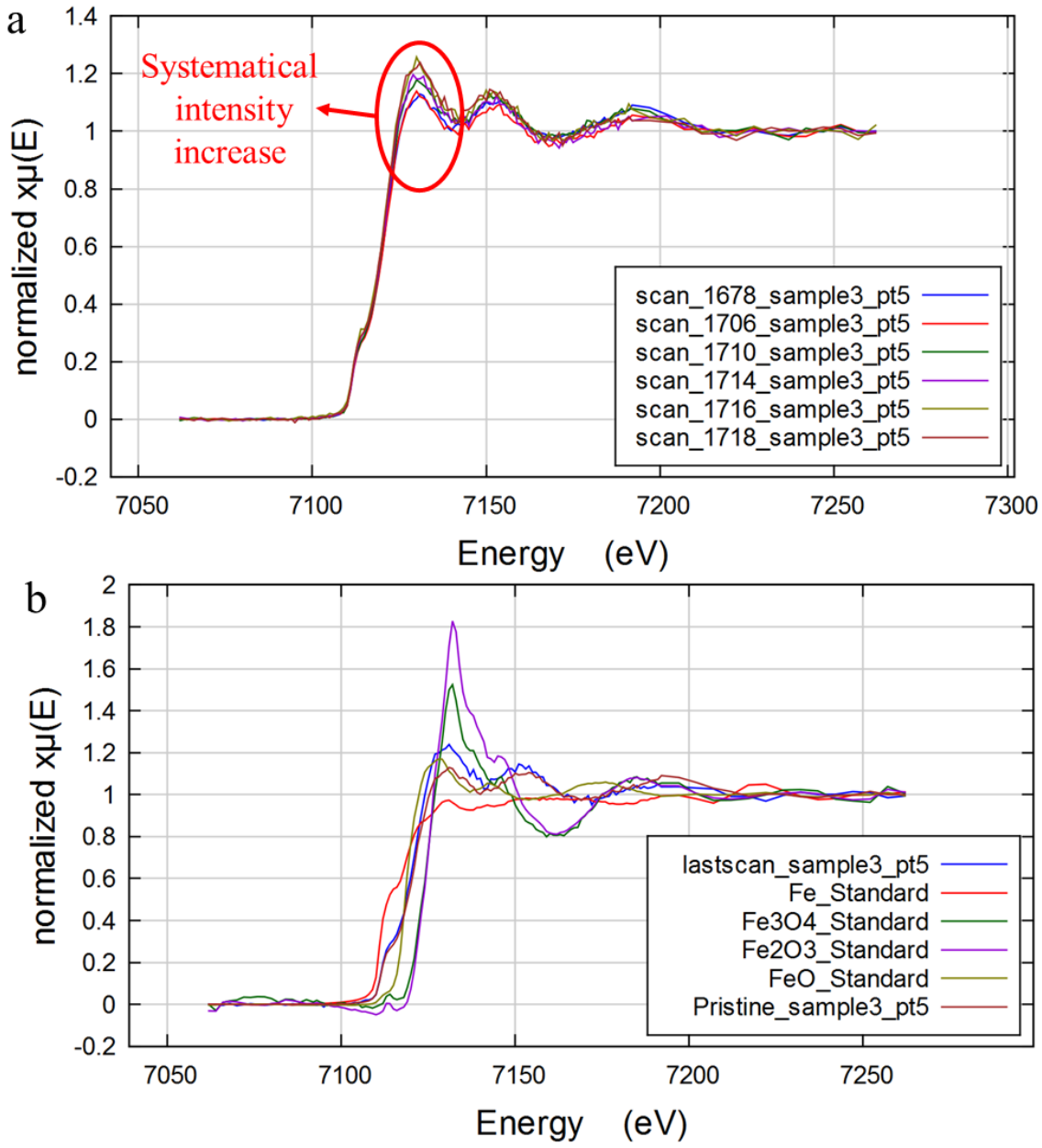

Figure 18 a. XANES scans showed systematical intensity increase of sample 3 point 5. b. Pristine and last XANES scan of sample 3 point 5 compared with standards.

In **Error! Reference source not found.**b, it shows the comparison of the sample (before/after treatment) and the standards. By comparing the last scan and pristine scan, pre-edge structure and white peak had slight shift, and the white line peak intensity increased. It's difficult

to determine the oxidation status of Fe, where more measurements need to be carried out both on the treated sample and other standards. Combined with the XRF mapping result, it's evident that the surface-treatment process can effectively prevent the corrosion. The fact that the XANES spectra differs from Fe (0) indicates a chemical reaction occurred between the Fe and coating materials during the surface treatment process, which may attribute to this anti-corrosion capability.

3.4 Conclusion

In situ investigation of surface morphology and chemical evolution of steel corrosion was successfully conducted. For sample 2 which is steel without coating, oxidation evolution was successfully detected by both XRF and XANES. XRF mapping showed morphological changes and concentration reduction in Fe, Cr, and Mn, XANES indicated a continuous oxidation from Fe (0) until a nearly complete oxidation. For sample 3 which is steel with anti-corrosion coating (Zr-based surface treatment, Henkel Corporation), only spectra taken from point 5 indicate some slow oxidation behavior started after approximately 12 hours treatment. XRF Fe mapping and XANES spectra from point 4 did not show evident changes. Thus, the surface treatment prevents the steel from corrosion effectively, with an apparent new layer of compound formation on the surface of the steel. The *in situ* cell was proven to be effective in conducting *in situ* investigation experiments, and could be used for further exploration. This experiment laid foundation for possibility in doing *in situ* research on numerous materials under various environments.

References

1. Adhikari, S., et al., Hexafluorozirconic acid based surface pretreatments: Characterization and performance assessment. Electrochimica Acta, 2011. 56(4): p. 1912-1924.
2. Als-Nielsen, J. and D. McMorrow, Elements of modern x-ray physics. 2011: WILEY.
3. Wille, K., Synchrotron radiation sources, in Engines of Discovery - A Century of Particle Accelerators. 2014, World Scientific Publishing Company. p. 161-198.
4. Toraldo di Francia, G., Introduction to the theory of synchrotron radiation, in Rendiconti della Scuola Internazionale di Fizika Enrico Fermi. Corso XII: Varenna Summer School on Solar Radioastronomy. 1960, Zanichelli.
5. Kunz, C., Introduction-properties of synchrotron radiation, in Synchrotron radiation. Techniques and applications, C. Kunz, Editor. 1979, Springer-Verlag. p. 1-23.
6. Buras, B., R. Fourme, and M.H.J. Koch, X-ray diffraction principles and applications, in Handbook on synchrotron radiation, E.E. Koch, Editor. 1983, North-Holland. p. 1015-1090.
7. Ding-Shyue, Y., L. Changshi, and A.H. Zewail, 4D electron diffraction reveals correlated unidirectional behavior in zinc oxide nanowires. Science, 2008. 321(5896): p. 1660-4.
8. Joo, J., et al., Face-selective electrostatic control of hydrothermal zinc oxide nanowire synthesis. Nature Materials, 2011. 10(8): p. 596-601.
9. Pu Xian, G., et al., Conversion of zinc oxide nanobelts into superlattice-structured nanohelices. Science, 2005. 309(5741): p. 1700-4.

10. Abutaha, A.I., S.R.S. Kumar, and H.N. Alshareef, Crystal orientation dependent thermoelectric properties of highly oriented aluminum-doped zinc oxide thin films. Applied Physics Letters, 2013. 102(5).
11. Kim, H., et al., Transparent conducting aluminum-doped zinc oxide thin films for organic light-emitting devices. Applied Physics Letters, 2000. 76(3): p. 259-261.
12. Pern, F.J., et al. Damp-Heat Induced Degradation of Transparent Conducting Oxides for Thin-Film Solar Cells. in 33rd IEEE Photovoltaic Specialists Conference. 2008. San Diego, CA.
13. Steinhauser, J., et al., Humid environment stability of low pressure chemical vapor deposited boron doped zinc oxide used as transparent electrodes in thin film silicon solar cells. Thin Solid Films, 2011. 520(1): p. 558-562.
14. Theelen, M., et al., Physical and chemical degradation behavior of sputtered aluminum doped zinc oxide layers for Cu(In,Ga)Se-2 solar cells. Thin Solid Films, 2014. 550: p. 530-540.
15. Schrauben, J.N., et al., Titanium and Zinc Oxide Nanoparticles Are Proton-Coupled Electron Transfer Agents. Science, 2012. 336(6086): p. 1298-1301.
16. Zhong Lin, W. and S. Jinhui, Piezoelectric nanogenerators based on zinc oxide nanowire arrays. Science, 2006. 312(5771): p. 242-6.
17. Yong, Q., W. Xudong, and W. Zhong Lin, Microfibre-nanowire hybrid structure for energy scavenging. Nature, 2008. 451(7180): p. 809-813.
18. Qiu, Y., et al., Direct current sputtered aluminum-doped zinc oxide films for thin crystalline silicon heterojunction solar cell. Materials Chemistry and Physics, 2013. 141(2-3): p. 744-751.

19. Calnan, S., et al., High deposition rate aluminium-doped zinc oxide films with highly efficient light trapping for silicon thin film solar cells. Thin Solid Films, 2008. 516(6): p. 1242-1248.

20. Tabassum, S., et al., Damp heat stability of AZO transparent electrode and influence of thin metal film for enhancing the stability. Journal of Materials Science-Materials in Electronics, 2014. 25(7): p. 3203-3208.

21. Hupkes, J., et al., Damp heat stability and annealing behavior of aluminum doped zinc oxide films prepared by magnetron sputtering. Thin Solid Films, 2006. 511-512: p. 673-7.

22. Greiner, D., et al., Damp heat stability of Al-doped zinc oxide films on smooth and rough substrates. Thin Solid Films, 2011. 520(4): p. 1285-1290.

23. Hupkes, J., et al., Damp heat stable doped zinc oxide films. Thin Solid Films, 2014. 555: p. 48-52.

24. Lemire, H.M., et al. Degradation of transparent conductive oxides; Mechanistic insights across configurations and exposures. in Conference on Reliability of Photovoltaic Cells, Modules, Components, and Systems VI. 2013. San Diego, CA.

25. Lee, D.W., et al., Effects of ZnO:Al films on CIGS PV modules degraded under accelerated damp heat. Solar Energy Materials and Solar Cells, 2012. 105: p. 15-20.

26. Greiner, D., et al., Influence of damp heat on the optical and electrical properties of Al-doped zinc oxide. Thin Solid Films, 2009. 517(7): p. 2291-2294.

27. Dhakal, T.P., et al., Moisture-Induced Surface Corrosion in AZO Thin Films Formed by Atomic Layer Deposition. Ieee Transactions on Device and Materials Reliability, 2012. 12(2): p. 347-356.

28. Kim, J.I., et al., Quantitative analyses of damp-heat-induced degradation in transparent conducting oxides. Solar Energy Materials and Solar Cells, 2014. 122: p. 282-286.

29. Tabassum, S., et al., Sol-gel and rf sputtered AZO thin films: analysis of oxidation kinetics in harsh environment. Journal of Materials Science-Materials in Electronics, 2014. 25(11): p. 4883-4888.

30. Tohsophon, T., et al., Damp heat stability and annealing behavior of aluminum doped zinc oxide films prepared by magnetron sputtering. Thin Solid Films, 2006. 511: p. 673-677.

31. Chang, S.H., Y.L. Wei, and H.P. Wang, Zinc species distribution in EDTA-extract residues of zinc-contaminated soil. Journal of Electron Spectroscopy and Related Phenomena, 2007. 156: p. LVII-LVII.